Voltage-dependent activation in EAG channels follows a ligand-receptor rather than a mechanical-lever mechanism

Received for publication, January 22, 2019, and in revised form, February 21, 2019 Published, Papers in Press, February 26, 2019, DOI 10.1074/jbc.RA119.007626

Olfat A. Malak[‡1], Grigory S. Gluhov[§2], Anastasia V. Grizel[¶], Kseniya S. Kudryashova[§‖], Olga S. Sokolova[§3], and Gildas Loussouarn[‡3,4]

From the [‡]INSERM, CNRS, l'Institut du Thorax, Université de Nantes, 44007 Nantes, France, the [§]Moscow M.V. Lomonosov State University, Moscow 119234, Russia, the [¶]Saint Petersburg State University, Saint Petersburg 199034, Russia, and the [‖]Shemyakin-Ovchinnikov Institute of Bioorganic Chemistry of Russian Academy of Sciences, Moscow 117997, Russia

Edited by Roger J. Colbran

Ether-a-go-go family (EAG) channels play a major role in many physiological processes in humans, including cardiac repolarization and cell proliferation. Cryo-EM structures of two of them, K_V10.1 and human ether-a-go-go-related gene (hERG or K_V11.1), have revealed an original nondomain-swapped structure, suggesting that the mechanism of voltage-dependent gating of these two channels is quite different from the classical mechanical-lever model. Molecular aspects of hERG voltage-gating have been extensively studied, indicating that the S4-S5 linker (S4-$S5_L$) acts as a ligand binding to the S6 gate (S6 C-terminal part, $S6_T$) and stabilizes it in a closed state. Moreover, the N-terminal extremity of the channel, called N-Cap, has been suggested to interact with S4-$S5_L$ to modulate channel voltage-dependent gating, as N-Cap deletion drastically accelerates hERG channel deactivation. In this study, using COS-7 cells, site-directed mutagenesis, electrophysiological measurements, and immunofluorescence confocal microscopy, we addressed whether these two major mechanisms of voltage-dependent gating are conserved in K_V10.2 channels. Using cysteine bridges and S4-$S5_L$–mimicking peptides, we show that the ligand/receptor model is conserved in K_V10.2, suggesting that this model is a hallmark of EAG channels. Truncation of the N-Cap domain, Per-Arnt-Sim (PAS) domain, or both in K_V10.2 abolished the current and altered channel trafficking to the membrane, unlike for the hERG channel in which N-Cap and PAS domain truncations mainly affected channel deactivation. Our results suggest that EAG channels function via a conserved ligand/receptor model of voltage gating, but that the N-Cap and PAS domains have different roles in these channels.

Voltage-gated potassium (K_V) channels regulate a variety of cellular processes, including membrane polarization (1, 2), apoptosis (3), cell proliferation (4), and cell volume (5). In connection with such a variety of functions of K_V channels, mutations in these channels cause a variety of pathological conditions in humans: neurological disorders (6, 7), cardiac arrhythmias (2), multiple sclerosis (8), and pain syndrome (9). It has also been shown that K_V channels are associated with the development of malignant tumors cancer (10). K_V10 channels belong to the ether-a-go-go family (EAG),[5] as hERG channels. Two isoforms of K_V10 channels are expressed in mammals: K_V10.1 (eag1) and K_V10.2 (eag2), which show 70% amino acid sequence identity. K_V10.1 has been detected mainly in the brain, whereas K_V10.2 is also expressed in other tissues such as the skeletal muscles, heart, placenta, lungs, and liver (11).

Atomic structures of rat K_V10.1 (12) and human hERG (K_V11.1) channels (13) highlighted many structural similarities: nonswapped pore and voltage domains, *i.e.* facing voltage-sensor and pore domains are from the same subunit, short S4-S5 linkers (S4-$S5_L$) and similar N-terminal structures such as Per-Arnt-Sim (PAS) and N-Cap domains. We hypothesized that molecular mechanisms of gating identified in hERG may apply to the closely related K_V10 channels.

In the heart, deactivation of hERG channels (closing of the activation gate) is slow, allowing a major role for this channel in the late repolarization phase of the action potential. In this channel, two mechanisms have been shown to play a major role in the deactivation process.

First, hERG deactivation is due to a voltage-dependent interaction between the S4-S5 region, including the S4-S5 linker and a part of S5 (named S4-$S5_L$, Fig. 1*A*) and the C-terminal part of the S6 segment (named here $S6_T$), which is the activation gate (14, 15). In other words, at resting potentials, S4-$S5_L$ (the ligand) is bound to the $S6_T$ gate (the receptor) and locks it in a closed state (as shown in Fig. 1*B*, *left*). Upon membrane depolarization, S4 drags S4-$S5_L$ out of the $S6_T$ gate, and the channel

This work was supported by Kolmogorov program of the Partenariat Hubert Curien Grant 35503SC (to G. L. and O. A. M.), Ministry of Education and Science of Russian Federation Grant RFMEFI61615X0044 (to O. S. S. and G. S. G.), a Fondation Genavie (to O. A. M.), Postdoctoral Fellowship 1.50.1038.2014 from St. Petersburg State University and a grant from the Dynasty Foundation (to A. G.). The authors declare that they have no conflicts of interest with the contents of this article.

This article contains Figs. S1–S3.

[1] Laureate of the Line Pomaret-Delalande prize of Fondation pour la Recherche Médicale Grant PLP20141031304. Present address: Cardiovascular Institute, Stanford University, 300 Pasteur Dr., Stanford, CA 94305-5111.

[2] Russian Scientific Foundation Laureate of Young Investigator Award 18-74-00087.

[3] Both authors contributed equally to this work.

[4] To whom correspondence should be addressed: L'institut du thorax, INSERM UMR 1087/CNRS UMR 6291, IRS-UN, 8 Quai Moncousu BP 70721, 44007 Nantes cedex 1, France. Tel.: 33-0-2-2808-0150; E-mail: gildas.loussouarn@inserm.fr.

[5] The abbreviations used are: EAG, ether-a-go-go; PAS, Per-Arnt-Sim; WGA, wheat germ agglutinin; DAPI, 4′,6-diamidino-2-phenylindole; $tbHO_2$, tert-butylhydroperoxide; EGFP, enhanced green fluorescent protein.

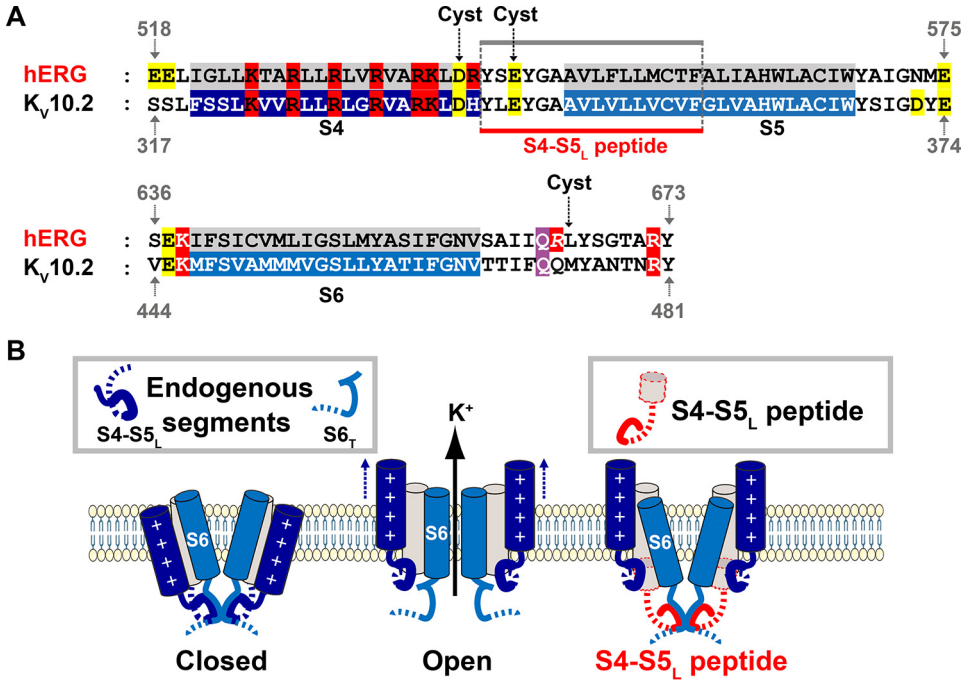

Figure 1. Alignment used to design the cysteine mutants and the S4-S5$_L$ peptide, hypothetical ligand/receptor model. *A*, alignment between hERG and K$_V$10.2. This alignment was used to (i) introduce the cysteines in S4-S5$_L$ and S6$_T$ and (ii) design the S4-S5$_L$ peptide from the previously identified hERG S4-S5$_L$ inhibiting peptide. S4-S5$_L$ refers to the S4-S5 region, including the S4-S5 linker and a part of S5. S6$_T$ refers to the C-terminal part of the S6 segment, which is the activation gate. The alignment was obtained using Cobalt (43). In *red* are represented the basic residues, in *yellow* acidic residues, and in *purple* the position of the narrowest part of the bundle crossing, also the gating residue (44). The *color boxes* represent the transmembrane segments. Introduced cysteines in hERG (15) and K$_V$10.2 in the present study are indicated. *Gray line* represents the inhibiting S4-S5$_L$ peptide in hERG (15). *Red line* represents the peptide engineered in K$_V$10.2 for the present study. *B,* left: scheme of the hypothetical ligand/receptor model in which S4-S5$_L$ (*deep blue*) binds to S6$_T$ (*light blue*) to stabilize the channel in a closed state. *Middle,* upon membrane depolarization, S4 pulls S4-S5$_L$ out of the S6$_T$ receptor, allowing channel opening. *Right,* the K$_V$10.2 S4-S5$_L$ peptide (*red*) mimics endogenous S4-S5$_L$, locking the channel in its closed conformation.

opens (Fig. 1*B*, *middle*). Upon repolarization S4-S5$_L$ binds to the S6$_T$ gate and channel deactivates (back to Fig. 1*B*, *left*). Here, using two distinct approaches, we observe that this ligand/receptor mechanism, which we originally proposed for hERG, is conserved in K$_V$10.2 (15).

Second, hERG deactivation is modulated by the channel N terminus. In the N-terminal eag domain, deletion in the N-Cap and/or the PAS domains, profoundly accelerated deactivation with no major effect on maximal current amplitude (16–19). Moreover, covalent binding of the N-Cap and the S4-S5$_L$ closed the channel (20). These observations suggested that the N-Cap and/or the PAS domains regulate channel deactivation by modulating S4-S5$_L$ and S6$_T$ interaction. In K$_V$10.2, we show that the eag domain presents quite different functions. Deletions of the N-Cap and PAS domains, separately or altogether, completely abolish channel activity, at least partially due to a defect in membrane trafficking.

In conclusion, we show that slowing activating channels follow an allosteric model, in which the voltage sensor and pore domains are weakly coupled, via a ligand, S4-S5$_L$ and a receptor, S6$_T$. In K$_V$10.2, such coupling is not modulated by the eag domain, as proposed for hERG (20).

Results

As in hERG, covalent binding of S4-S5$_L$ to S6$_T$ locks the K$_V$10.2 channel closed

The similar structures of hERG and K$_V$10.1 (12, 13) showing a nonswapped arrangement of the pore and voltage sensor domains suggest that voltage-gating of these channels does not follow the classical mechanical-lever model in which S4-S5$_L$ constricts the S6$_T$ gate (21). Also, functional evidence obtained by several groups including ours, strongly suggests that hERG channels do not follow the mechanical-lever model (14, 15). First, Ferrer and collaborators, observed that introduction of a cysteine in S4-S5$_L$ (D540C) and another cysteine in S6$_T$ (L666C) locks the channel in a closed state in oxidative conditions. This was associated to a restricted movement of the voltage sensor in a oxidative condition, as measured by gating currents, suggesting the formation of a disulfide bridge (14). Also, mutagenesis experiments on hERG suggested electrostatic interaction between Asp-540 and Leu-666 playing a major role in hERG voltage-dependent gating (22). Such observations suggest that in the WT hERG channel, specific interactions between S4-S5$_L$ and the activation gate (S6$_T$) stabilize the closed channel. In transfected COS-7 cells, we could reproduce the experiments originally done by Ferrer and collaborators (14) in the *Xenopus* oocyte model. Moreover we could observe that a S4-S5$_L$ mimicking peptide inhibits the hERG channel, suggesting a ligand/receptor model, in which S4-S5$_L$, directly under the control of the voltage sensor S4, binds to S6$_T$ to lock the channel in a closed state (see Fig. 1*B*, *right*).

To check whether K$_V$10.2 channels follow the same voltage-gating mechanism as hERG channels, we aligned the amino acid sequences of the two channels, and mutated to a cysteine Asp-339 and Met-474 in K$_V$10.2, corresponding to hERG positions in which cysteines were previously introduced: Asp-540 in

S4-S5$_L$ and Leu-666 in S6$_T$ (14, 15) (*black arrows* in Fig. 1*A*). As for the hERG double cysteine mutant, a 2-h application of 0.2 mM tert-butylhydroperoxide ($tbHO_2$) led to an almost complete inhibition of the D339C/M474C K_V10.2 channel current (Fig. 2, *A* and *B*). Knowing the high homology between hERG and K_V10.2 (65%), we supposed that D339C and M474C in K_V10.2 also form a disulfide bridge in oxidative conditions, as a cause of the drastic current reduction. As control experiments, 0.2 mM $tbHO_2$ application had no effect on tail current amplitude when only one (D339C or M474C K_V10.2) or none (WT K_V10.2) of the two cysteines was introduced (Fig. 2, *C–H*) and activation curves showed a similar shift in all conditions (Fig. S1). Because a 2-h $tbHO_2$ application represents a slow time course for a putative disulfide bridge formation, we also applied a higher concentration of $tbHO_2$ (2 mM) for a shorter time. As in the Ferrer study (14) on hERG, this concentration led, in around 12 min, to an almost complete inhibition of the D339C/M474C K_V10.2 channel current but not the WT channel current (Fig. 3). This inhibition was reversed by 10 mM DTT, as in the Ferrer study on hERG (14).

To strengthen the hypothesis of the interaction between S4-S5$_L$ and S6$_T$ in K_V10.2, we also tested the $tbHO_2$ effect on another double mutant of the K_V10.2 channel. We chose the E343C/M474C K_V10.2 channel, because Glu-343, in S4-S5$_L$, is aligned with Glu-544 in hERG, which when mutated to a cysteine together with L666C in hERG S6$_T$ (Fig. 1*A*), also lead to channel inhibition, suggesting the formation of a disulfide bridge (15). We observed an inhibition of the current after 15 min incubation of 2 mM $tbHO_2$, which is reversed by 10 mM DTT (Fig. 4, *A* and *B*). Control experiments showed no effect either on tail current amplitude or on the activation curve when only one (E343C or M474C K_V10.2) or none (WT K_V10.2) of the two cysteines was introduced (Fig. 4, *C–H*, Fig. S2). Altogether, these observations confirmed that two different disulfide bridges created between the two introduced cysteines in S4-S5$_L$ and S6$_T$ locks K_V10.2 in a closed state, as in hERG (14, 15).

As in hERG, a K_V10.2 S4-S5$_L$ mimicking peptide inhibits K_V10.2 channels

Recently, we observed that (i) co-expressing a hERG S4-S5$_L$ mimicking peptide with hERG channel partially inhibited the generated current and (ii) covalently binding this peptide to the hERG channel completely inhibited it (15). These observations suggest that in hERG channels, S4-S5$_L$ rather acts as a voltage-controlled ligand that binds to the S6$_T$ gate and stabilizes it in the closed state (Fig. 1*B*, *left*, for the endogenous interaction and *B*, *right*, for the mimicking peptide). This mechanism of gating is consistent with Ferrer *et al.* (14) observation that covalent binding of S4-S5$_L$ and S6$_T$ channel regions locks the channel in a closed state. Using the alignment between hERG and K_V10.2 (Fig. 1*A*), we designed the K_V10.2 S4-S5$_L$ peptide from the position of the S4-S5$_L$ peptide sequence that was inhibiting the hERG channel (15). Co-expressing the K_V10.2 channel with its specific S4-S5$_L$ peptide led to a profound decrease in current density (more than 70%), with no shift in the activation curve, as observed for hERG (Fig. 5, *A–E*). As an additional control, co-expressing K_V10.2 with a scramble S4-S5$_L$ peptide led to current density similar to the one observed in the absence of peptide (Fig. 5, *A* and *B*).

Because the S4-S5$_L$ peptide is supposed to interfere with the gating, it may be intriguing that activating and tail currents are inhibited to the same extent, and that neither the activation curve, nor the activation kinetics are modified (Fig. 5, *C–F*). To address this issue, we used a kinetic model mimicking channel activity in the presence/absence of the peptide (Fig. 6), based on a previous model of KCNE1–KCNQ1 and S4-S5$_L$ peptide interaction (23). In the KCNE1–KCNQ1 model, the presence of the peptides was affecting the channel activation curve and activation kinetics. However, when constrained to K_V10.2 kinetics, the model did not show any alteration of activation kinetics or steady-state activation (Fig. 6, *B* and *C*). This is because peptide binding and unbinding rates (0.02 and 0.04 s^{-1}, respectively) are lower than channel opening/closing rates, because increasing these rates leads to alterations in channel activation kinetics and steady-state activation (Fig. 6, *B* and *C*). A peptide with similar binding/unbinding rates impact KCNE1–KCNQ1 channel activation curve and activation kinetics (23) because gating kinetics of this channel are slower than K_V10.2 kinetics. Altogether, these observations support the ligand/receptor model of voltage dependence in K_V10 channels.

As opposed to hERG, N-Cap and PAS domain-deleted K_V10.2 channels are not functional

The results described above suggest that in both K_V10.2 and hERG channels, deactivation is due to S4-S5$_L$ binding to S6$_T$ and consequent stabilization of the closed state. It has been shown by several works that intracellular N-cap and PAS domains of hERG (shown in Fig. 7*A* for K_V10.2, *cf.* alignment in Fig. S3) modulate channel deactivation kinetics. Most importantly truncated hERG channels missing N-Cap or the whole eag domain (N-Cap + PAS), when expressed in *Xenopus* oocytes, showed robust currents but a more than 5-fold acceleration in deactivation (16–19). Also in mammalian cells, it has been observed that the eag domain is not necessary for hERG channel trafficking, consistent with the observation of robust currents in this model (24, 25). Another work showed that N-Cap is close to S4-S5$_L$ (20). Thus, N-Cap may modulate channel deactivation through a direct interaction with this linker. Based on all these observations, we supposed that deletion of both N-Cap and PAS domains in K_V10.2 should give rise to functional channels with accelerated deactivation, as in the study on hERG in mammalian cells (25). Transfection of WT K_V10.2 tagged with 1D4 at the C terminus gave rise to a current similar to a previous description (6) and immunofluorescence experiments using this tag showed plasma membrane enrichment of the channel, compared with the intracellular compartment (Fig. 7, *B–F*). Surprisingly, deletion of N-Cap domain, PAS domain, but also of both domains all resulted in nonfunctional K_V10.2 channels (Figs. 8*B*, 9*B*, and 10*B*). Immunofluorescence experiments on N-Cap and/or PAS domains truncated channels showed no membrane enrichment of the channels (Figs. 8, *C–F*, 9, *C–F*, and 10, *C–F*). These findings

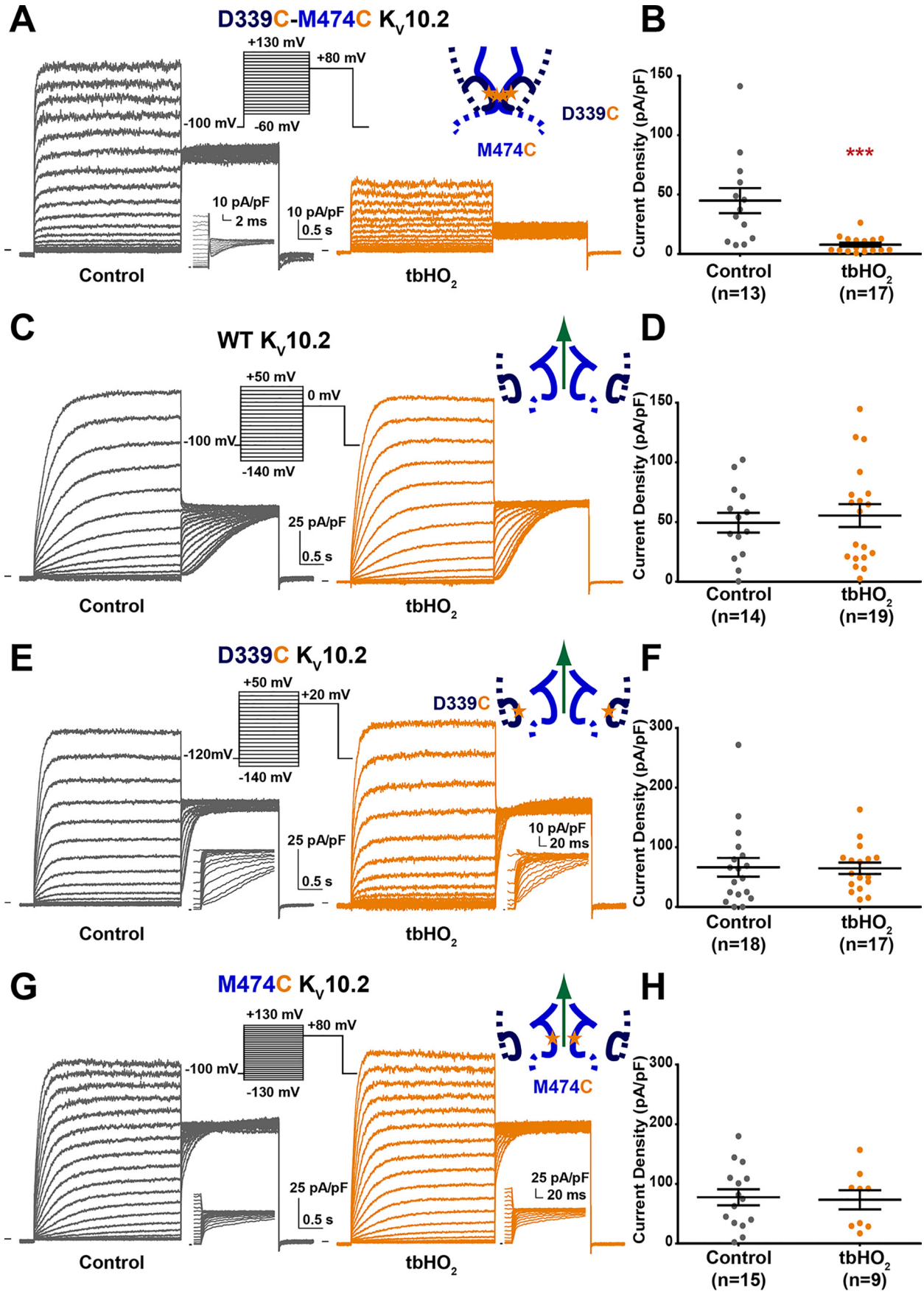
A
D339C-M474C K$_V$10.2
+130 mV
+80 mV
-100 mV
-60 mV
D339C
M474C
10 pA/pF
2 ms
10 pA/pF
0.5 s
Control
tbHO$_2$
B
Current Density (pA/pF)
150
100
50
0
***
Control
(n=13)
tbHO$_2$
(n=17)
C
WT K$_V$10.2
+50 mV
0 mV
-100 mV
-140 mV
25 pA/pF
0.5 s
Control
tbHO$_2$
D
Current Density (pA/pF)
150
100
50
0
Control
(n=14)
tbHO$_2$
(n=19)
E
D339C K$_V$10.2
+50 mV
+20 mV
D339C
-120mV
-140 mV
25 pA/pF
0.5 s
10 pA/pF
20 ms
Control
tbHO$_2$
F
Current Density (pA/pF)
300
200
100
0
Control
(n=18)
tbHO$_2$
(n=17)
G
M474C K$_V$10.2
+130 mV
+80 mV
-100 mV
-130 mV
M474C
25 pA/pF
0.5 s
25 pA/pF
20 ms
Control
tbHO$_2$
H
Current Density (pA/pF)
300
200
100
0
Control
(n=15)
tbHO$_2$
(n=9)

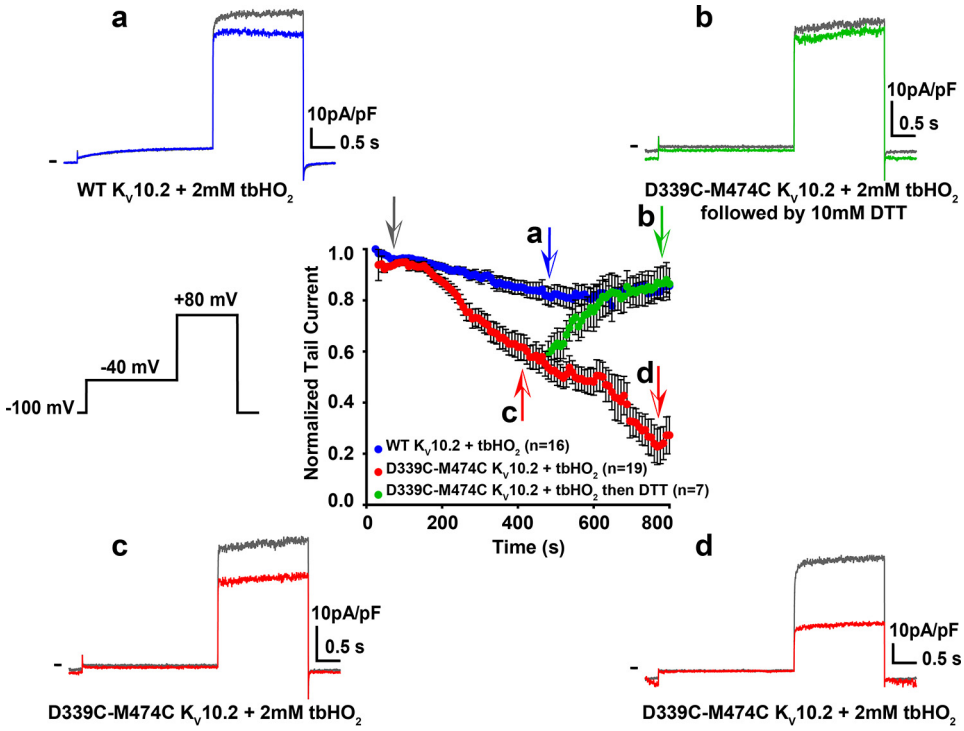

Figure 3. Kinetics of D339C/M474C K_V10.2 current reduction upon addition of 2 mM $tbHO_2$. Time course of the effect of $tbHO_2$ application on normalized WT and D339C/M474C K_V10.2 tail currents. From a holding potential of −100 mV, followed by a 3-s prepulse at −40 mV, tail currents were recorded at +80 mV, every 8 s. Following stabilization of the tail current, 2 mM $tbHO_2$ was perfused (*gray arrow*), and the step protocol was repeated for 6 min. Following the $tbHO_2$ application, a fraction of the cells was then perfused with 10 mM DTT, and the step protocol was continued for an additional 6 min. Each data point represents the mean ± S.E. current magnitude normalized to values obtained before $tbHO_2$, n = 16 (WT), 19 (D339C/M474C in $tbHO_2$), and 7 (D339C/M474C in DTT). *Insets* (*a–d*) correspond to representative recordings at the *arrows*.

suggest a trafficking defect of the N-Cap and/or PAS domains truncated Kv10.2 channels.

As opposed to hERG, coexpressing a K_V10.2 N-Cap mimicking peptide with truncated K_V10.2 does not counteract the effect of channel truncation

For the hERG channel, it has been shown that a peptide corresponding to the first 16 amino acids of the channel is sufficient to reconstitute slow deactivation to hERG lacking this region (19). Similarly, another study has shown that injection of the purified eag domain, corresponding to the first 135 amino acids of hERG, into oocytes expressing eag-truncated hERG, restores the deactivation kinetics to WT-like in more than 24 h (17). Based on these previous observations on hERG, we proposed that co-expression of specific K_V10.2 N-Cap mimicking peptides with the N-Cap–truncated K_V10.2 channel should recover its expression and activity at the plasma membrane. Surprisingly again, K_V10.2 channel activity was not recovered in the presence of N-Cap mimicking peptide (n = 8). This observation further suggests that N-Cap and PAS domains play distinct roles in hERG and K_V10.2 function.

Co-expression of WT and truncated K_V10.2 channels gives rise to a right shift in the activation curve as compared with homomeric WT channels, but no change in deactivation kinetics

To evaluate the potential effects of N-Cap truncation on channel activity, we co-expressed K_V10.2 missing the N-Cap with the WT channel, in an attempt to generate heteromers. We observed robust voltage-dependent currents, showing a ~30-mV shift in the activation curve toward depolarized potential, demonstrating the generation of such heteromers (Fig. 11, *C–F*). This shift in the activation curve suggests that N-Cap deletion leads not only to a K_V10.2 trafficking defect but also to a gating defect. In the hERG channel, deletion of N-Cap did not lead to a shift of the activation curve, but an acceleration of deactivation (26). In the present experiments on K_V10.2, no change in deactivation kinetics was observed when the N-Cap–truncated channel was co-expressed with the WT channel (Fig. 12). We also co-expressed the K_V10.2 channel construct lacking both the N-Cap and PAS domains, with the WT channel. Again, we observed a ~30-mV shift in the activation curve toward depolarized potentials, but no modification in deactivation (Figs. 11 and 12). Thus, although we are likely recording the

Figure 2. Introduction of 2 cysteines in the S4-$S5_L$ and $S6_T$ regions of K_V10.2 (D339C/M474C K_V10.2) locks the channel closed in oxidative conditions. *A*, representative, superimposed recordings of the D339C/M474C K_V10.2 current after 2 h incubation in Tyrode without (control) or with 0.2 mM $tbHO_2$ ($tbHO_2$). *Left inset,* activation voltage protocol used (one sweep every 8 s). *Right inset,* scheme of S4-$S5_L$/$S6_T$ with introduced cysteines (*stars*). *B*, mean ± S.E. D339C/M474C K_V10.2 maximum tail-current density, in control or $tbHO_2$. ***, $p < 0.001$ *versus* control, Mann-Whitney test. *C* and *D,* same as *A* and *B* for WT K_V10.2. *E* and *F,* same as *A* and *B* for D339C K_V10.2. *G* and *H,* same as *A* and *B* for M474C K_V10.2.

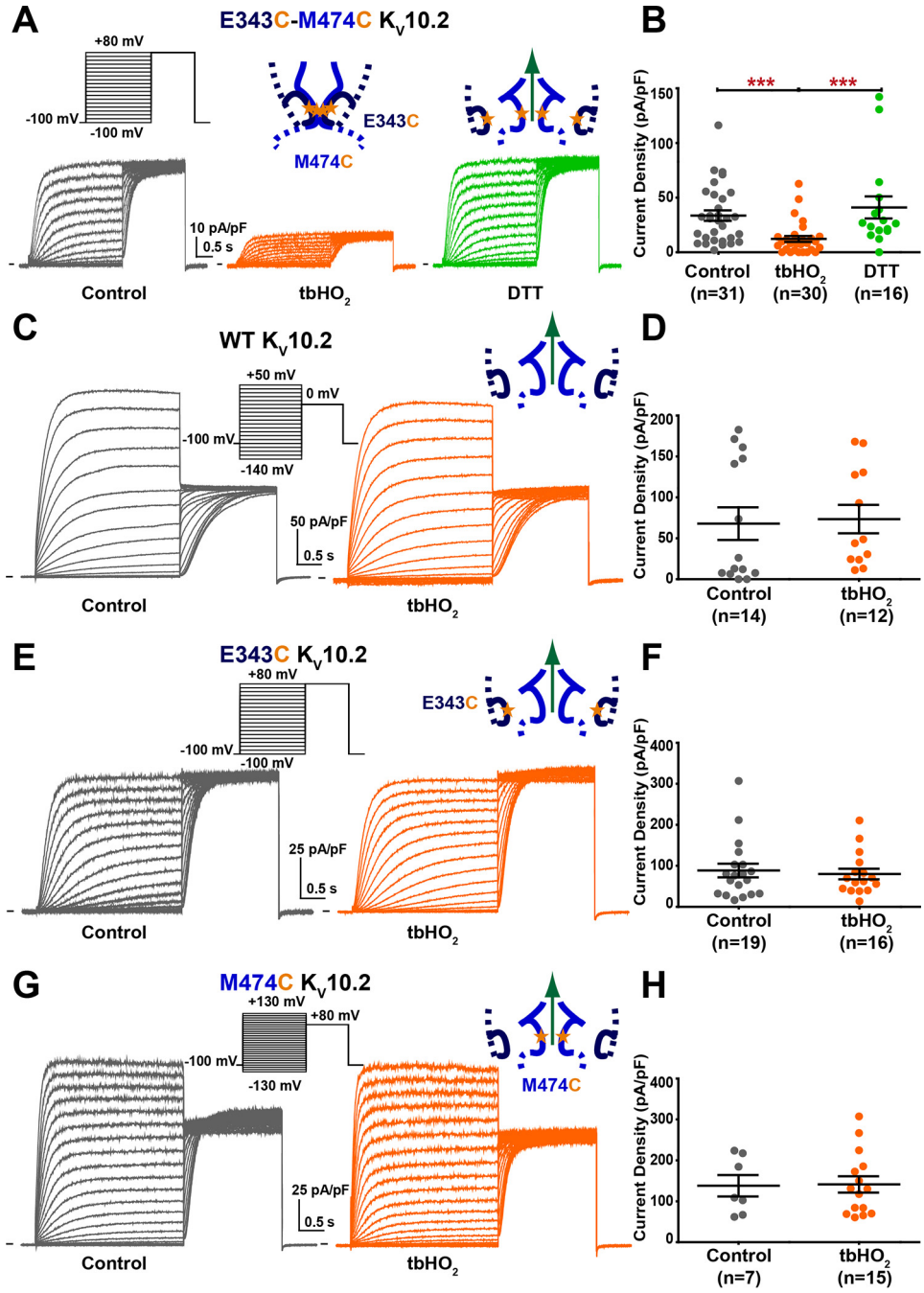

Figure 4. Introduction of 2 cysteines in the S4-S5$_L$ and S6$_T$ regions of K$_V$10.2 (E343C/M474C K$_V$10.2) locks the channel closed in oxidative conditions. *A,* representative, superimposed recordings of the E343C/M474C K$_V$10.2 current after 15 min incubation in Tyrode without (control) or with 2 mM tbHO$_2$ (*tbHO$_2$*), or after a subsequent 5-min incubation in 10 mM DTT. *Left inset,* activation voltage protocol used (one sweep every 8 s). *Middle* and *right insets,* schemes of S4-S5$_L$/S6$_T$ with introduced cysteines in the presence of tbHO$_2$ or DTT, respectively (*stars*). *B,* mean ± S.E. E343C/M474C K$_V$10.2 maximum tail-current density, in control, tbHO$_2$, or tbHO$_2$ followed by DTT. ***, $p < 0.001$, Mann-Whitney test. *C* and *D,* same as *A* and *B* for WT K$_V$10.2. *E* and *F,* same as *A* and *B* for E343C K$_V$10.2. *G* and *H,* same as *A* and *B* for M474C K$_V$10.2.

combined activities of tetrameric channels containing different ratios of the WT and truncated subunits, it appears that N-terminal deletion of K$_V$10.2 impacts the steady-state activation curve rather than deactivation kinetics.

Discussion

From the present and previous works, we suggest that among voltage-gated channels, coupling between voltage sensor movement and pore gating falls into two categories: (i) the mechanical-lever model: an obligatory coupling in which the S4 resting state directly translates into S6 gate-closed state. This mechanical-lever model, inferred from structural data in Shaker-like channels (27), also applies to eukaryotic sodium channels, as suggested by recent structural studies (28, 29); (ii) the ligand/receptor model: the obligatory coupling cannot hold if the S6$_T$ gate is able to open, even if S4 segments are in the resting state, as shown for hERG and KCNQ1 channels (30–32), and, vice versa, if the S6$_T$ gate is able to close, even if S4

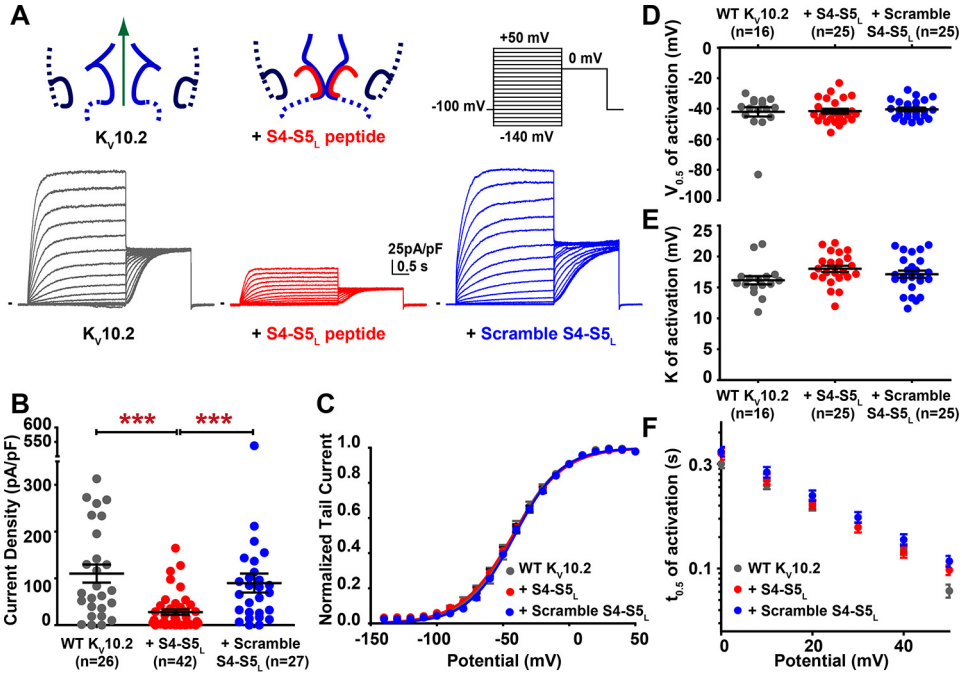

Figure 5. S4-S5$_L$ peptide inhibits K_V10.2 channels. *A,* representative, superimposed recordings of the WT K_V10.2 current in the absence (*left*; 2 μg of K_V10.2 plus 2 μg of GFP encoding plasmids), in the presence of S4-S5$_L$ peptide (*middle*; 2 μg of K_V10.2 plus 2 μg of peptide encoding plasmids), and in the presence of a scramble S4-S5$_L$ peptide (*right*; 2 μg of K_V10.2 plus 2 μg of peptide encoding plasmids). *Left insets*: schemes of the hypothetical effect of the S4-S5$_L$ inhibiting peptide on K_V10.2 channel; *right inset*: activation voltage protocol used (one sweep every 8 s). *B,* mean ± S.E. K_V10.2 maximum tail-current density in the absence or presence of the indicated peptide (S4-S5$_L$ peptide or scramble S4-S5$_L$ peptide). ***, $p < 0.001$, Mann-Whitney test. *C,* activation curve, obtained from tail currents using the protocol shown in *A*, in the absence or presence of the indicated peptide (n = 16–25). *D,* mean ± S.E. half-activation potential in the absence or presence of the indicated peptide. *E,* mean ± S.E. activation curve slope in the absence or presence of the indicated peptide. *F,* mean ± S.E. half-activation time as a function of membrane potential, in the absence or presence of the indicated peptide.

segments are in the activated state (33). We recently demonstrated this ligand/receptor model in hERG channels by using several approaches. Here, we obtained similar results on K_V10.2 using similar approaches.

First, introduction of cysteines in S4-S5$_L$ and S6$_T$ lock the channel in a closed state in oxidative conditions, suggesting the formation of a disulfide bridge, as in hERG. This suggests that the same gating mechanism applies to K_V10.2. Introduction of cysteines in both S4-S5$_L$ and S6$_T$ may lead to a nonnative conformation that favor an S4-S5$_L$ interaction with S6$_T$, which would not be met in the WT channel. But in the second set of experiments, a S4-S5$_L$ mimicking peptide, without any introduced cysteine, inhibits K_V10.2 channel, also without any introduced cysteine, further suggesting the capability of S4-S5$_L$ to stabilize the channel closed state. Noteworthy, similar channel-specific peptides have the same effect in KCNQ1 and hERG channels (15, 23). Complementary experiments in hERG revealed that S4-S5$_L$ peptide effects was on channel gating, and not channel trafficking (15).

Altogether these experiments suggest that K_V10.2 follows the ligand/receptor mechanism observed in hERG. In both channels, S4-S5 linkers are short (12, 13), thus it is likely that the part of S5 that is present in the peptide also plays a role in closed channel stabilization. Further structural data of hERG and K_V10.2 channels in the closed state should clarify the residues involved in the S4-S5$_L$ and S6$_T$ interaction. Noteworthy, this ligand/receptor model is consistent with the observation that the voltage-dependent closure of the related K_V10.1 channel, but also of the hERG channel, requires at least a part of the inhibiting S4-S5$_L$ to be covalently linked to the voltage sensor S4 (34, 35).

As opposed to similar ligand/receptor gating mechanisms in the two channels, the role of the eag domain (N-Cap + PAS) is quite different between hERG and K_V10.2. In hERG channels, the eag domain (N-Cap + PAS) is not necessary for channel activity and mainly modulates the current deactivation rate (17–19). Here, we observed that truncation of the K_V10.2 eag domain renders the channel nonfunctional, at least partly due to trafficking defects. In rescue experiments with the WT channel, we observed that eag domain deletion or even only N-Cap deletion are associated with a shift in the activation curve, but no change in channel deactivation. The contrary is observed in hERG channel: an altered deactivation, no shift in the activation curve (26, 36). Our results suggest major differences in functional roles for the N-Cap and PAS domains between K_V10.2 and hERG. Altogether, this work suggests a conserved ligand/receptor (allosteric) model of voltage gating, but divergent roles in eag domains among channels of the EAG family.

In combination with previous work on hERG, this study highlights the voltage-gated channels superfamily, divergent gating mechanisms (obligatory *versus* allosteric) that matches divergent structures (swapped *versus* nonswapped domain, respectively) and divergent kinetics (fast *versus* slow activating channels, respectively). Nonswapped domains (hERG, K_V10) may provide less contact between S4-S5$_L$ and S6$_T$ (12, 13). We

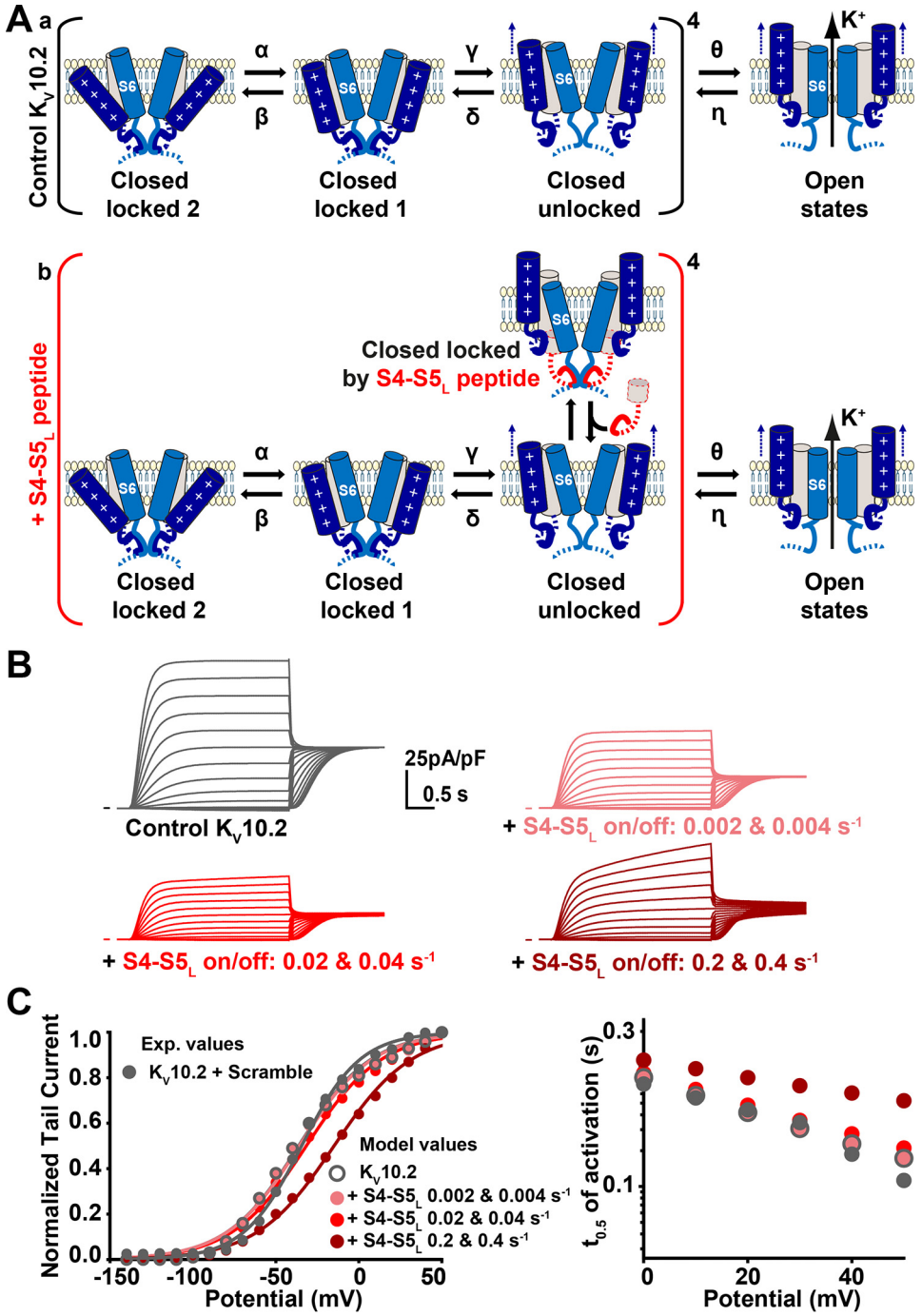

Figure 6. Kinetic model of K_V10.2 and its interaction with the S4-S5$_L$ peptide. *A,* kinetic model schemes. This model is based on a previous work on KCNE1-KCNQ1 (23). *a,* kinetic model in the absence of peptide, on which optimization has been performed (see "Experimental procedures"). Optimized transition rates are presented in Table 1. *b,* binding of exogenous S4-S5$_L$ locks the channel and prevents its opening. Peptides are supposed to interact with each monomer in the unlocked states. *B,* simulated currents during step protocols (same as in Fig. 5), in the absence (*Ctrl*) or presence of S4-S5$_L$ peptide, at the indicated S4-S5$_L$ on/off rates. *C, gray filled circles*: experimental activation curves and half-activation times in control condition. Other symbols: simulated values in the absence of peptide (control, *open circles*), or in the presence of peptides, at the indicated rates of peptide binding/unbinding.

propose that this weak coupling between S4-S5$_L$ and S6$_T$ provides a framework for a two-step channel activation: first, the fast S4 movement drags the ligand S4-S5$_L$ out of its receptor on the S6$_T$ gate, followed by slow gate opening. This allosteric regulation of the S6$_T$ gate by S4-S5$_L$ may explain how in slowly activating channels, movement of S4 is not concomitant to pore opening (37).

Experimental procedures

Plasmid constructs

pCDNA6 hK_V10.2 was subcloned into pMT3 vector using the standard PCR overlap extension method (38). A 1D4 immunoaffinity tag (derived from the C terminus of bovine rhodopsin) was added to the C terminus of all constructs (39). The D339C, E343C, M474C, E343C/M474C, and D339C/M474C

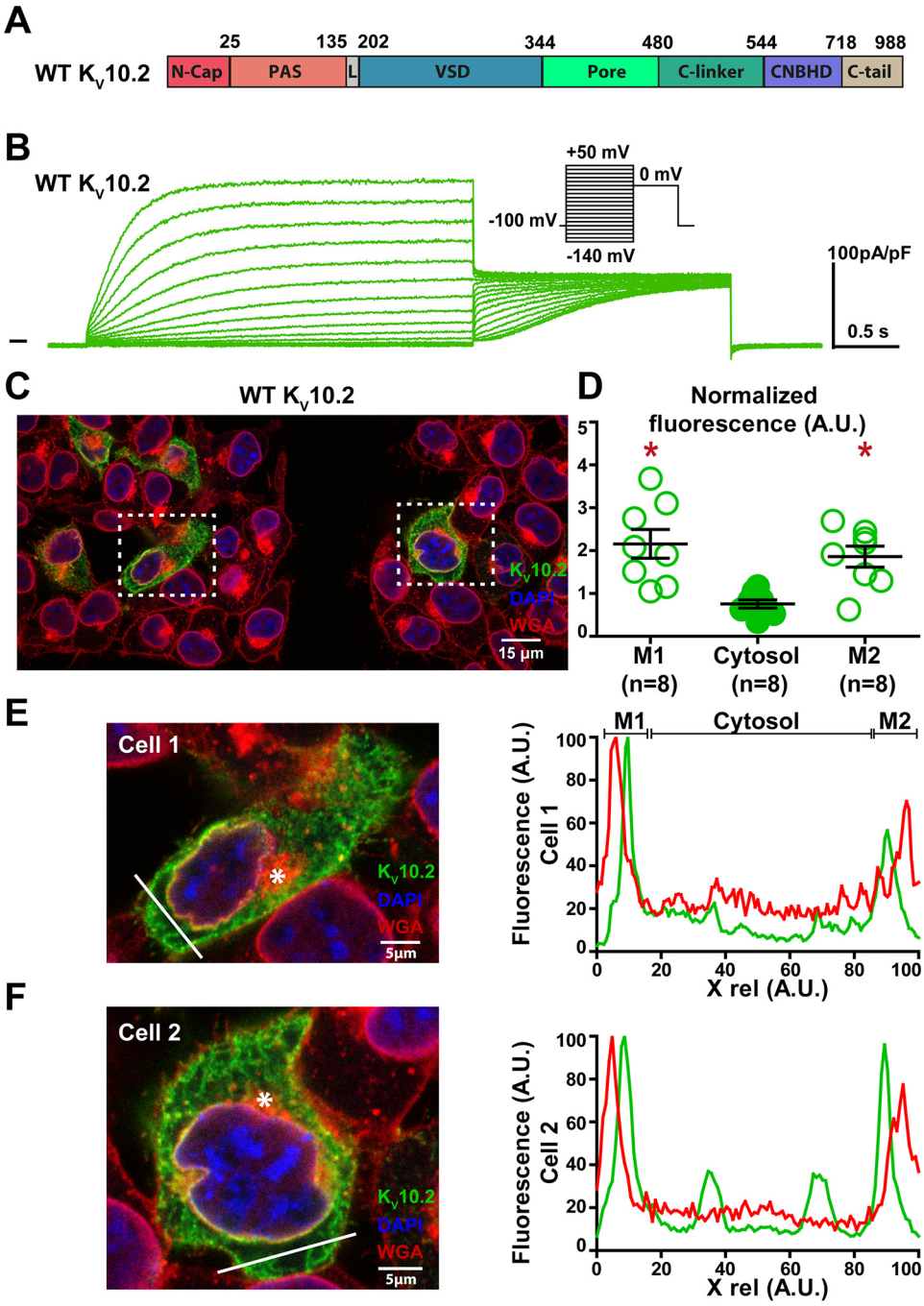

Figure 7. WT K$_V$10.2 characterization in transfected COS-7 cells. *A,* domain organization of the channel, showing the eag domain (N-Cap + PAS), a linker domain (L, also named proximal N terminus), the voltage-sensing domain (*VSD*), the pore domain, C-linker, CNBHD, and C-tail. *B,* representative, superimposed recordings of the WT K$_V$10.2–1D4 current. *Inset*: voltage protocol used (one sweep every 8 s). *C,* representative confocal immunostainings of WT K$_V$10.2–1D4 in transfected COS-7 cells (in *green*). WGA is used as a membrane marker (in *red*). Nuclei are stained with DAPI (in *blue*). *Scale bar* = 15 µm. *D,* mean ± S.E. fluorescence of K$_V$10.2 signal in plasma membrane (*M1* and *M2*) and cytosol, as measured in *E* and *F*, normalized by the average K$_V$10.2 fluorescence. *, $p < 0.05$ *versus* cytosol, paired Student's *t* test. *E* and *F, left:* expanded view of two selected cells, showing the Golgi (*stars*) and the line used for the line plots shown at the *right*. Lines have been placed as far as possible from the Golgi to generate accurate plasma membrane plots. *Right:* line plots of WGA (*red*) and K$_V$10.2 (*green*) at the level of the drawn lines at the *left*. Higher K$_V$10.2 fluorescence densities are observed in the region of the plasma membrane.

mutations were inserted into the pMT3-K$_V$10.2 construct using the QuikChange™ site-directed mutagenesis-based technique using Accuprime Pfx polymerase (ThermoFisher Scientific) according to the standard protocol recommended by the manufacturer. Truncation mutants were constructed by deleting residues 2 to 24 (ΔN-CAP), 2 to 134 (Δeag), and 25 to 134 (ΔPAS) using the standard PCR overlap extension method. PCR products were digested with HindIII and XbaI and ligated into pCDNA6 and PMT3 vectors. All constructs were confirmed by sequencing. Oligonucleotides encoding K$_V$10.2 peptides were synthesized by TOP Gene Technologies and contained a XhoI restriction enzyme, followed by a methionine (ATG) for translation initiation, a glycine (GGA) to protect the ribosome-binding site during translation, and the nascent pep-

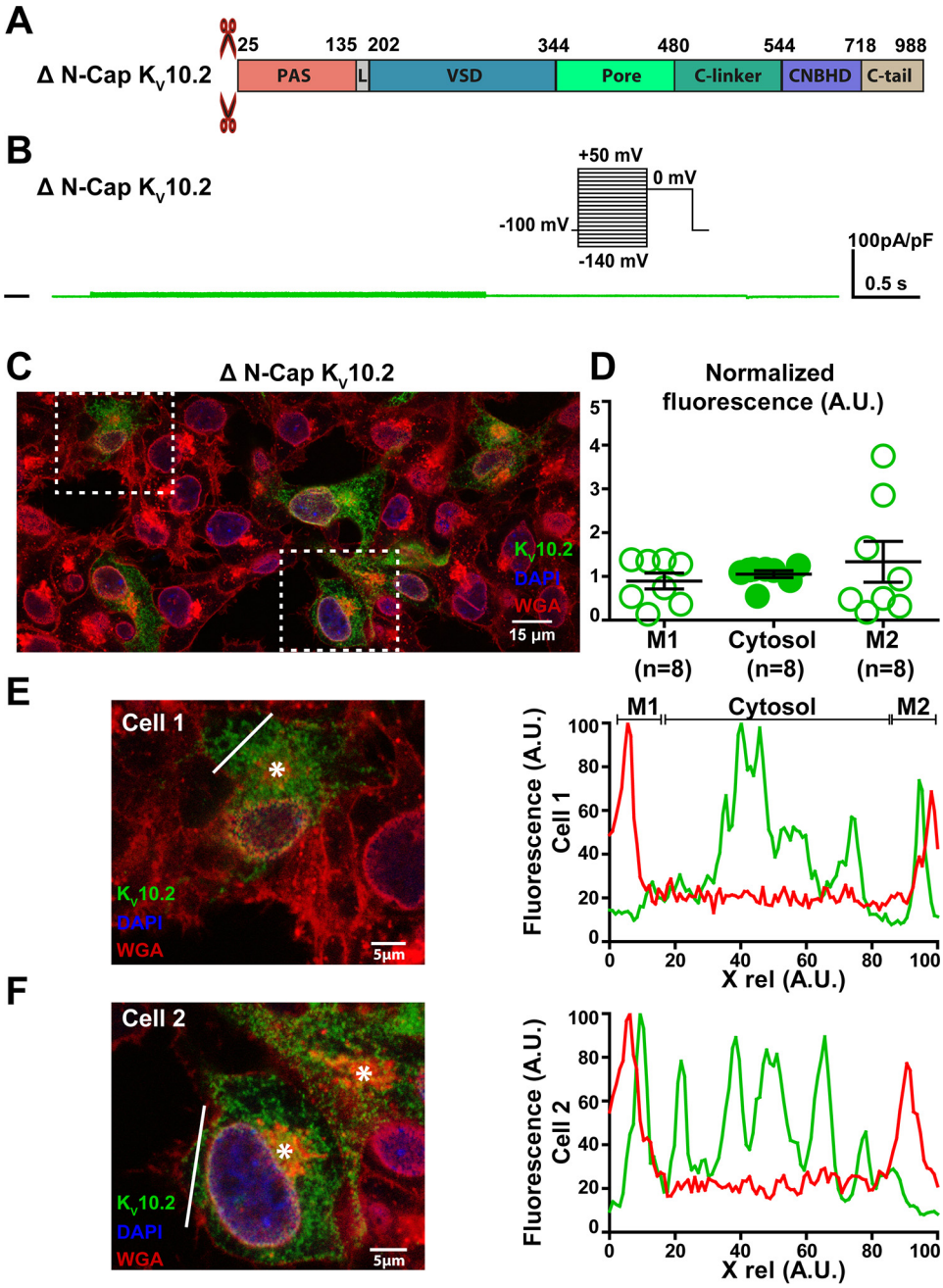

Figure 8. ΔN-Cap K_V10.2 characterization in transfected COS-7 cells. *A,* domains organization of the channel, showing the N-Cap deletion. *B,* representative, superimposed recordings of the ΔN-Cap K_V10.2–1D4 current. *Inset*: voltage protocol used (one sweep every 8 s). *C,* representative confocal immunostainings of ΔN-Cap K_V10.2–1D4 in transfected COS-7 cells (in *green*). WGA is used as a membrane marker (in *red*). Nuclei are stained with DAPI (in *blue*). *Scale bar* = 15 μm. *D*, mean ± S.E. fluorescence of the K_V10.2 signal in plasma membrane (M1 and M2) and cytosol, as measured in *E* and *F*, normalized by the average K_V10.2 fluorescence. *E* and *F, left:* expanded view of two selected cells, showing the Golgi (*stars*) and the line used for the line plots shown on the *right*. Lines have been placed as far as possible from the Golgi to generate accurate plasma membrane plots. *Right:* line plots of WGA (*red*) and K_V10.2 (*green*) at the level of the drawn lines at the *left*. Higher K_V10.2 fluorescence densities are not observed in the region of the plasma membrane, as opposed to the WT condition.

tide against proteolytic degradation (40). A BamHI restriction enzyme site was synthesized at the 3′ end immediately following the translational stop codon (TGA). These oligonucleotides were then ligated into pIRES2-EGFP (Clontech) and sequenced.

Cell culture and transfection

The African green monkey kidney-derived cell line COS-7 was obtained from the American Type Culture Collection (CRL-1651) and cultured in Dulbecco's modified Eagle's medium (GIBCO) supplemented with 10% fetal calf serum and antibiotics (100 IU/ml penicillin and 100 μg/ml of streptomycin) at 5% CO_2 and 95% air, maintained at 37 °C in a humidified incubator. Cells were transfected in 35-mm Petri dishes when the culture reached 50–60% confluence, with 4 μg of total DNA complexed with 12 μl of FuGENE-6 (Roche Molecular Biochemical) according to the standard protocol recommended by the manufacturer. In different experiments, plas-

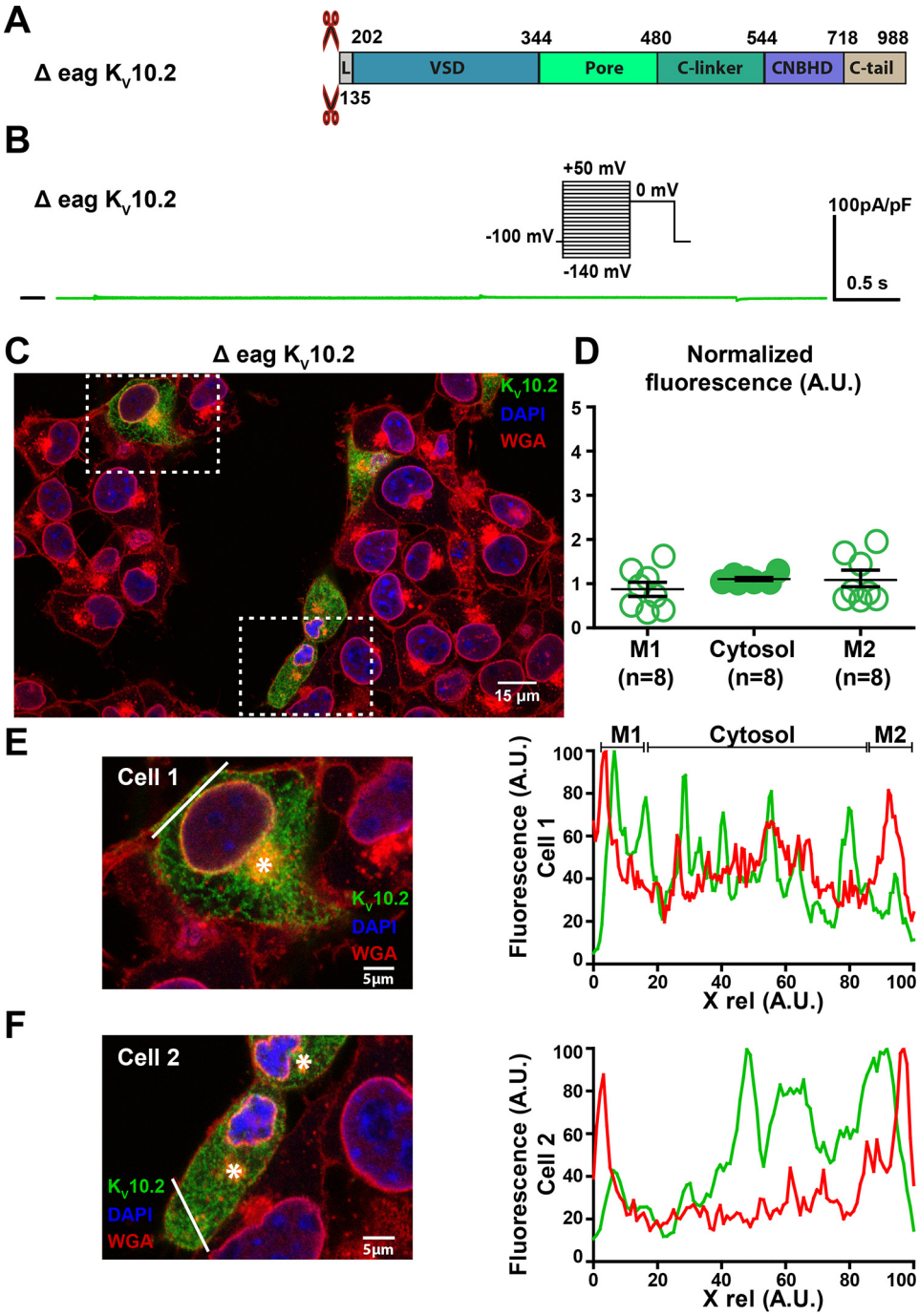

Figure 9. Δeag K$_V$10.2 characterization in transfected COS-7 cells. *A,* domains organization of the channel, showing the eag domain deletion. *B,* representative, superimposed recordings of the Δeag K$_V$10.2–1D4 current. *Inset*: voltage protocol used (one sweep every 8 s). *C,* representative confocal immunostainings of Δeag K$_V$10.2–1D4 in transfected COS-7 cells (in *green*). WGA is used as a membrane marker (in *red*). Nuclei are stained with DAPI (in *blue*). *Scale bar* = 15 μm. *D,* mean ± S.E. fluorescence of K$_V$10.2 signal in plasma membrane (*M1* and *M2*) and cytosol, as measured in *E* and *F*, normalized by the average K$_V$10.2 fluorescence. *E* and *F, left:* expanded view of two selected cells, showing the Golgi (*stars*) and the line used for the line plots shown at the *right*. Lines have been placed as far as possible from the Golgi to generate accurate plasma membrane plots. *Right:* line plots of WGA (*red*) and K$_V$10.2 (*green*) at the level of the drawn lines at the *left*. Higher K$_V$10.2 fluorescence densities are not observed in the region of the plasma membrane, as opposed to the WT condition.

mid quantities were optimized to keep current amplitudes in a range that undetectable currents were rare, and large currents inducing incorrect voltage-clamp were also rare. Immunofluorescence and confocal microscopy experiments were done with pCDNA6-K$_V$10.2 for which channel expression was lower than with pMT3-K$_V$10.2, to limit intracellular accumulation of the protein. For disulfide bridge experiments, COS-7 cells were co-transfected with 3.6 μg of pMT3-WT, D339C/M474C, E343C/M474C, D339C, E343C, M474C K$_V$10.2, and 0.4 μg of pEGFP. For S4-S5$_L$ peptide experiments, COS-7 cells were co-transfected with 2 μg of pMT3-WT K$_V$10.2 and 2 μg of pIRES2-EGFP plasmids encoding or not the S4-S5$_L$ peptide. As an additional control, a pIRES2-EGFP plasmid encoding a scramble S4-S5$_L$ peptide was used. In pIRES2-EGFP plasmids, the second cassette (EGFP) is less expressed than the first cassette, guaranteeing high levels of peptide expression in fluorescent cells

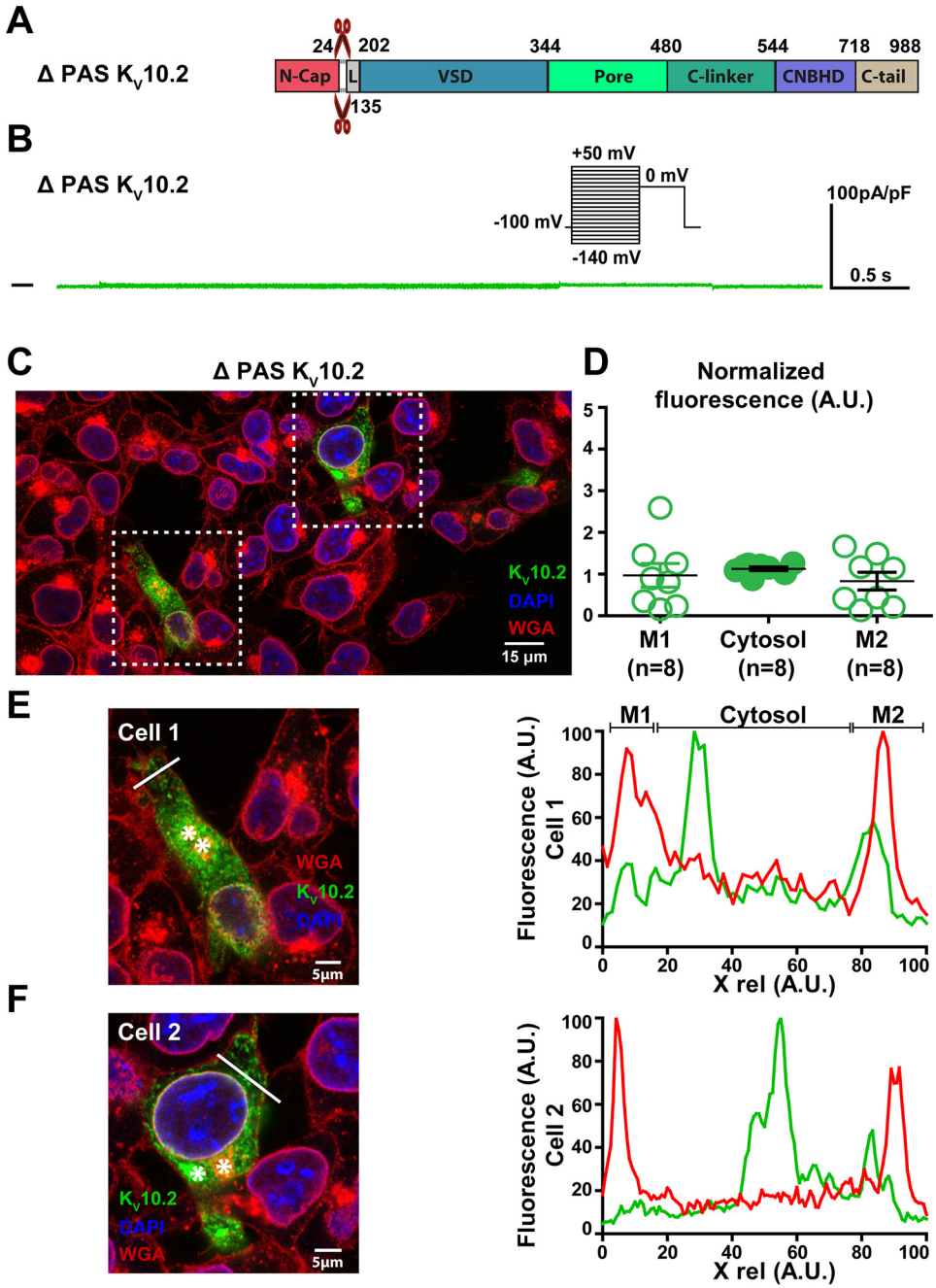

Figure 10. ΔPAS K_V10.2 characterization in transfected COS-7 cells. *A,* domains organization of the channel, showing the PAS domain deletion. *B,* representative, superimposed recordings of the ΔPAS K_V10.2–1D4 current. *Inset*: voltage protocol used (one sweep every 8 s). *C,* representative confocal immunostainings of ΔPAS K_V10.2–1D4 in transfected COS-7 cells (in *green*). WGA is used as a membrane marker (in *red*). Nuclei are stained with DAPI (in *blue*). *Scale bar* = 15 μm. *D,* mean ± S.E. fluorescence of K_V10.2 signal in plasma membrane (*M1* and *M2*) and cytosol, as measured in *E* and *F*, normalized by the average K_V10.2 fluorescence. *E* and *F, left:* expanded view of two selected cells, showing the Golgi (*stars*) and the line used for the line plots shown at the *right*. Lines have been placed as far as possible from the Golgi to generate accurate plasma membrane plots. *Right:* line plots of WGA (*red*) and K_V10.2 (*green*) at the level of the drawn lines at the *left*. Higher K_V10.2 fluorescence densities are not observed in the region of the plasma membrane, as opposed to the WT condition.

(23). For N-terminal deletion experiments, COS-7 cells were co-transfected with 2 μg of pCDNA6-N-Cap truncated K_V10.2 and 2 μg of pIRES2-EGFP plasmids encoding or not the N-Cap mimicking peptide. For immunofluorescence and confocal microscopy experiments, COS-7 cells were transfected with 4 μg of pCDNA6-WT/truncated K_V10.2. For WT/truncated heteromeric K_V10.2 experiments, COS-7 cells were co-transfected with 1.8 μg of pMT3-WT K_V10.2, 1.8 μg of pMT3-truncated K_V10.2, and 0.4 μg of pEGFP. Cells were re-plated onto 35-mm Petri dishes the day after transfection for patch clamp experiments.

Electrophysiology

One day after splitting, COS-7 cells were mounted on the stage of an inverted microscope and constantly perfused by a Tyrode solution (*cf.* below) at a rate of 1–3 ml/min. The bath

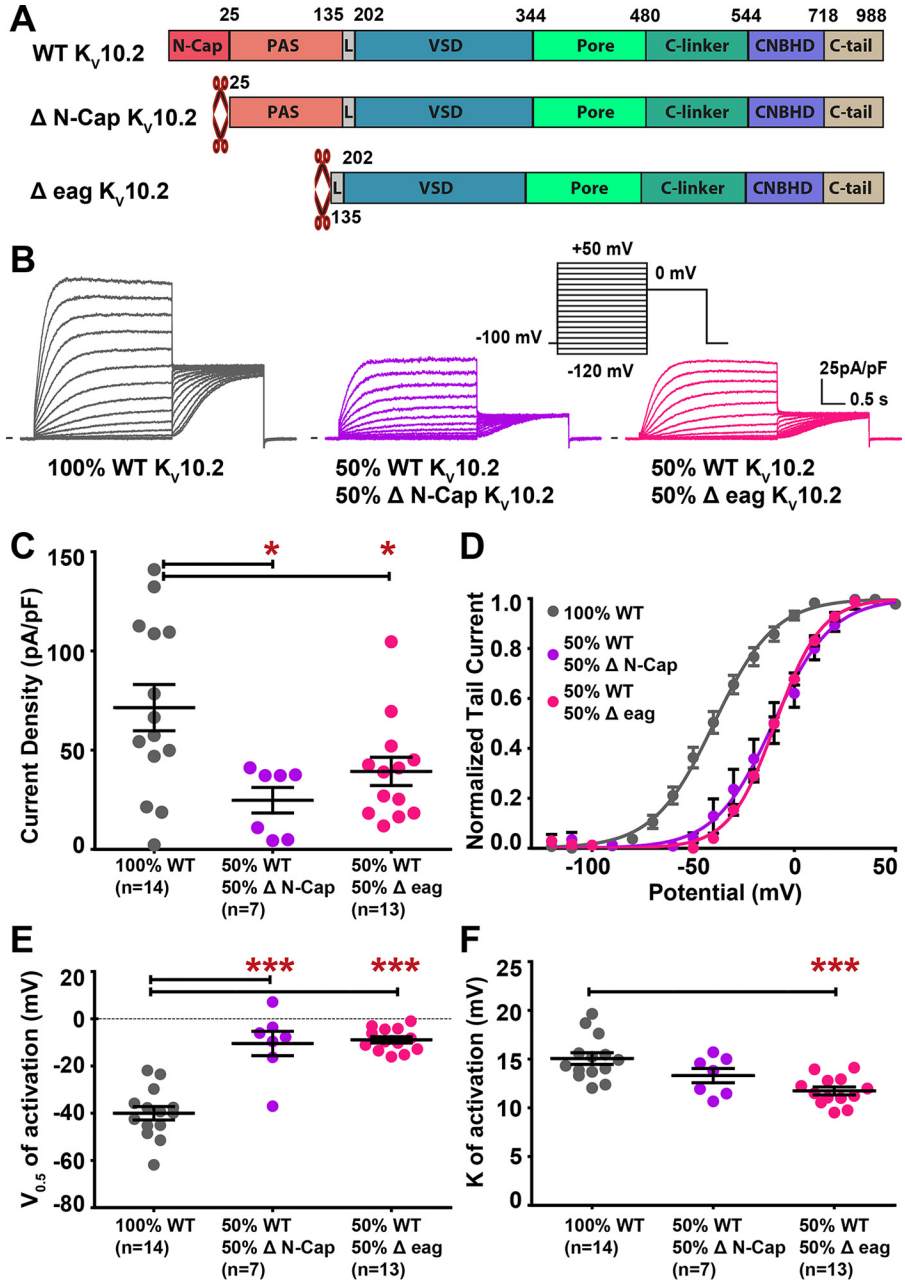

Figure 11. Co-expression of WT and truncated K$_V$10.2 channels uncovers a right shift in the activation curve, as compared with WT channel. *A,* domain organization of WT and truncated channels. *B,* representative, superimposed recordings of COS-7 cells transfected with WT K$_V$10.2 channel (*left*), WT and ΔN-Cap K$_V$10.2 (*middle*), and WT and Δeag K$_V$10.2 (*right*). *Inset,* activation voltage protocol used (one sweep every 8 s). *C,* mean ± S.E. K$_V$10.2 maximum tail-current density, in the indicated conditions. *, $p < 0.05$ *versus* WT, Mann-Whitney test. *D,* activation curve in the indicated conditions. *E,* mean ± S.E. half-activation potential (V$_{0.5}$). ***, $p < 0.001$ *versus* WT, Student's *t* test. *F,* mean ± S.E. activation slope (*k*). ***, $p < 0.001$ *versus* WT, Student's *t* test.

temperature was maintained at 22.0 ± 2.0 °C. Stimulation and data recording were performed with Axon pClamp 10, an A/D converter (Digidata 1440A), and an Axopatch 200B amplifier (all Molecular Devices). Patch pipettes (tip resistance: 2–3 megohms) were pulled from soda lime glass capillaries (Kimble-Chase) and coated with wax. Currents were recorded in the whole-cell configuration, pipette capacitance and series resistance were electronically compensated (by around 75%). Activation protocols were adjusted to the voltage-dependence of the construct as in the previous study on hERG (15). Activation curves were obtained from the tail currents and fitted by Boltzmann equations.

Confocal microscopy

Immunohistological analyses were performed to study cell localization of transfected WT/truncated K$_V$10.2–1D4 in COS-7 cells. Twenty-four hours after transfection, cells were plated on IBIDI plates for 24 h. Cells were then fixed with 4% formaldehyde, stained for 10 min at room temperature with Alexa Fluor™ 647 conjugated wheat germ agglutinin (WGA; ThermoFisher), a plasma membrane marker, permeabilized with 0.5% saponin and blocked with 1% PBS/BSA. Cells were then incubated with a mouse mAb directed against the 1D4 tag diluted in PBS (Abcam). Secondary antibody staining was per-

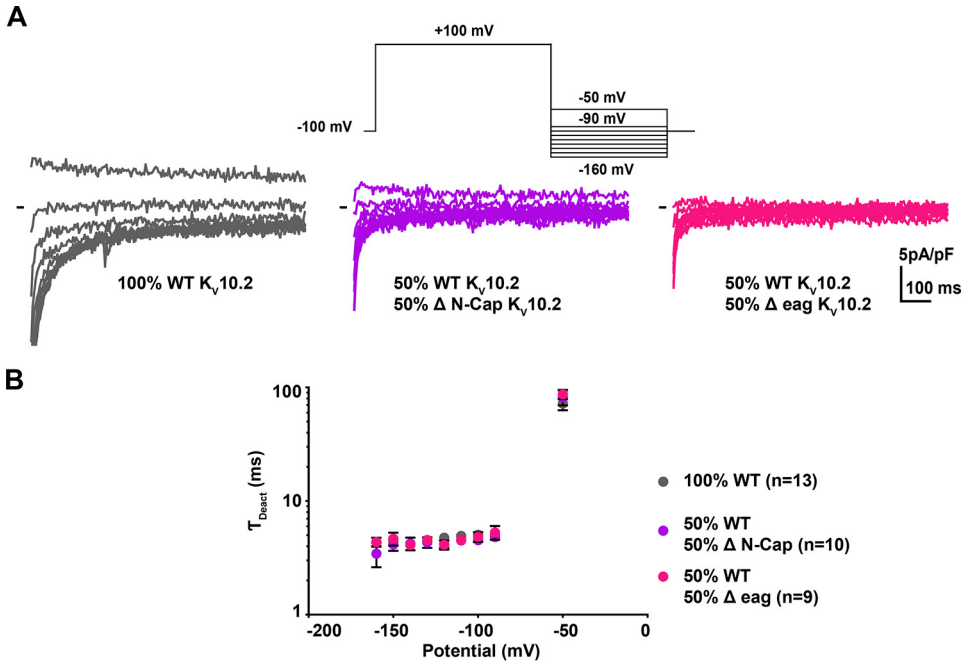

Figure 12. Co-expression of WT and truncated K_V10.2 channels is not associated with changes in deactivation kinetics, as compared with WT channel. *A,* representative, superimposed recordings of COS-7 cells transfected with WT K_V10.2 channel (*left*), WT and ΔN-Cap K_V10.2 (*middle*), and WT and Δeag K_V10.2 (*right*). *Upper inset*: deactivation tail voltage protocol used (prepulse duration, 3 s, one sweep every 7 s). *B,* mean ± S.E. K_V10.2 deactivation time constant, obtained from a monoexponential fit of the deactivating current.

Table 1

Optimized transition rates used in the model presented in Fig. 6

The abbreviations use are: F = 96485 C. mol^{-1} (Faraday constant); R = 8.314 J. $mol^{-1}.K^{-1}$ (gas constant); T = 297 K; V (membrane potential) in V.

Transition description		Transition rate (s^{-1})
Voltage sensor transition rates		
Closed Locked 2 (CL2) → Closed Locked 1 (CL1)	α	$8.50 \cdot \exp\left(0.14 \cdot \frac{V \cdot F}{R \cdot T}\right)$
CL1→ CL2	β	$13.35 \cdot \exp\left(-0.10 \cdot \frac{V \cdot F}{R \cdot T}\right)$
CL1 → Closed unlock (CU)	γ	$15.95 \cdot \exp\left(0.42 \cdot \frac{V \cdot F}{R \cdot T}\right)$
CU → CL1	δ	$4.12 \cdot 10^{-2} \cdot \exp\left(-0.76 \cdot \frac{V \cdot F}{R \cdot T}\right)$
Concerted opening transition rates		
4 monomers CU or CUP6 → Open state 1 (O1)	θ	$260.7 \cdot \exp\left(0.36 \cdot \frac{V \cdot F}{R \cdot T}\right)$
O1 → 4 monomers CU or CUP6	η	$64.66 \cdot \exp\left(-0.61 \cdot \frac{V \cdot F}{R \cdot T}\right)$
O1 → Open state 2 (O2)	ψ	$6.20 \cdot 10^{-3} \cdot \exp\left(2.37 \cdot \frac{V \cdot F}{R \cdot T}\right)$
O2 → O1	ω	$12.74 \cdot \exp\left(-2.46 \cdot \frac{V \cdot F}{R \cdot T}\right)$

formed using Alexa 488-conjugated anti-mouse antibody. DAPI was used for nuclear staining. Conventional imaging was performed using a LSM710-Confocor3 (Zeiss) and a Nikon Confocal A1RSi microscope system equipped with a SR Apo 100 × 1.49 N.A objective. Images were analyzed with ImageJ software. In figures, but not for analyses, Enhance Local Contrast adjustment was performed on WGA staining to highlight plasma membrane staining. To quantify fluorescence, the line plot was arbitrarily segmented in 3 different regions: the first and last 5–15% of the line plot, corresponding to plasma membrane (M1 and M2), and the remaining intermediate 70% of the line plot, corresponding to the intracellular compartment. For each of these regions in each cell, K_V10.2 fluorescence intensity values were normalized by the average cell K_V10.2 fluorescence intensity signal (41).

Solutions

Cells were continuously superfused with a HEPES-buffered Tyrode solution containing (in mmol/liter): NaCl 145, KCl 4, $MgCl_2$ 1, $CaCl_2$ 1, HEPES 5, glucose 5, pH adjusted to 7.4 with NaOH. Patch pipettes were filled with the following solution (in mmol/liter): KCl 100, K-gluconate 45, $MgCl_2$ 1, EGTA 5, HEPES 10, pH adjusted to 7.2 with KOH. For experiments in Fig. 3, 1 mM K_2ATP was added to limit current rundown. The membrane-permeable oxidizing agent $tbHO_2$ was obtained from Sigma. Incubation of COS-7 cells with 0.2 or 2 mM $tbHO_2$ was realized at room temperature.

Kinetic model

The K_V10.2 kinetic model (Fig. 6*A*, *top*) contains two voltage sensor transitions, and two open states, as in the model of I_{Ks} (42). This model was optimized using IChMASCOT (J.A. De Santiago-Castillo and M. Covarrubias) to fit traces of the representative control of Fig. 5. Optimized transition rates are presented in Table 1. Next, another model was designed (Fig. 6*A*, *bottom*), with an additional state in which S4-$S5_L$ mimicking peptide binds to the pre-open state and stabilizes it, as in Ref. 23. Various S4-$S5_L$ binding/unbinding transition rates were applied, and the effects on the biophysical parameters were studied.

Statistics

All data are expressed as mean ± S.E. Statistical differences between current densities (data points are not normally distributed) were determined using nonparametric Mann-Whitney test. Statistical differences between activation parameters, $V_{0.5}$, K (data points are normally distributed) were determined using unpaired Student's *t* tests. A value of $p < 0.05$ was considered significant.

Author contributions—O. A. M., O. S. S., and G. L. data curation; O. A. M., G. S. G., A. V. G., and K. S. K. formal analysis; O. A. M., O. S. S., and G. L. validation; O. A. M., G. S. G., A. V. G., K. S. K., O. S. S., and G. L. investigation; O. A. M., G. S. G., A. V. G., K. S. K., O. S. S., and G. L. methodology; O. A. M., O. S. S., and G. L. writing-original draft; O. A. M., O. S. S., and G. L. writing-review and editing; O. S. S. and G. L. conceptualization; O. S. S. and G. L. supervision; O. S. S. and G. L. funding acquisition; O. S. S. and G. L. project administration; G. L. resources.

Acknowledgments—We thank Isabelle Baró for careful reading of the manuscript. We thank the MicroPiCell facility of SFR Santé F. Bonamy for confocal microscopy experiments (Nantes). O. A. M. personally thanks Line Pomaret for her generous support. The LSM710-Confocor3 microscope was supported by the Moscow Lomonosov State University Program of Development.

References

1. Yellen, G. (2002) The voltage-gated potassium channels and their relatives. *Nature* **419,** 35–42 CrossRef Medline
2. Charpentier, F., Mérot, J., Loussouarn, G., and Baró, I. (2010) Delayed rectifier K^+ currents and cardiac repolarization. *J. Mol. Cell Cardiol.* **48,** 37–44 CrossRef Medline
3. Pal, S., Hartnett, K. A., Nerbonne, J. M., Levitan, E. S., and Aizenman, E. (2003) Mediation of neuronal apoptosis by Kv2.1-encoded potassium channels. *J. Neurosci.* **23,** 4798–4802 CrossRef Medline
4. Jiménez-Perez, L., Cidad, P., Álvarez-Miguel, I., Santos-Hipólito, A., Torres-Merino, R., Alonso, E., de la Fuente, M. Á., López-López, J. R., and Pérez-García, M. T. (2016) Molecular determinants of Kv1.3 potassium channels-induced proliferation. *J. Biol. Chem.* **291,** 3569–3580 CrossRef Medline
5. Piron, J., Choveau, F. S., Amarouch, M. Y., Rodriguez, N., Charpentier, F., Mérot, J., Baró, I., and Loussouarn, G. (2010) KCNE1-KCNQ1 osmoregulation by interaction of phosphatidylinositol-4,5-bisphosphate with Mg^{2+} and polyamines. *J. Physiol.* **588,** 3471–3483 CrossRef Medline
6. Yang, Y., Vasylyev, D. V., Dib-Hajj, F., Veeramah, K. R., Hammer, M. F., Dib-Hajj, S. D., and Waxman, S. G. (2013) Multistate structural modeling and voltage-clamp analysis of epilepsy/autism mutation Kv10.2-R327H demonstrate the role of this residue in stabilizing the channel closed state. *J. Neurosci.* **33,** 16586–16593 CrossRef Medline
7. Watanabe, H., Nagata, E., Kosakai, A., Nakamura, M., Yokoyama, M., Tanaka, K., and Sasai, H. (2000) Disruption of the epilepsy KCNQ2 gene results in neural hyperexcitability. *J. Neurochem.* **75,** 28–33 Medline
8. Judge, S. I., and Bever, C. T., Jr. (2006) Potassium channel blockers in multiple sclerosis: neuronal Kv channels and effects of symptomatic treatment. *Pharmacol. Ther.* **111,** 224–259 CrossRef Medline
9. Beekwilder, J. P., O'Leary, M. E., van den Broek, L. P., van Kempen, G. T., Ypey, D. L., and van den Berg, R. J. (2003) Kv1.1 channels of dorsal root ganglion neurons are inhibited by *n*-butyl-*p*-aminobenzoate, a promising anesthetic for the treatment of chronic pain. *J. Pharmacol. Exp. Ther.* **304,** 531–538 CrossRef Medline
10. Pardo, L. A., and Stuhmer, W. (2014) The roles of K^+ channels in cancer. *Nat. Rev. Cancer* **14,** 39–48 CrossRef Medline
11. Ju, M., and Wray, D. (2002) Molecular identification and characterisation of the human eag2 potassium channel. *FEBS Lett.* **524,** 204–210 CrossRef Medline
12. Whicher, J. R., and MacKinnon, R. (2016) Structure of the voltage-gated K^+ channel Eag1 reveals an alternative voltage sensing mechanism. *Science* **353,** 664–669 CrossRef Medline
13. Wang, W., and MacKinnon, R. (2017) Cryo-EM structure of the open human ether-a-go-go-related K^+ channel hERG. *Cell* **169,** 422–430 CrossRef Medline
14. Ferrer, T., Rupp, J., Piper, D. R., and Tristani-Firouzi, M. (2006) The S4-S5 linker directly couples voltage sensor movement to the activation gate in the human ether-a-go-go-related gene (hERG) K+ channel. *J. Biol. Chem.* **281,** 12858–12864 CrossRef Medline
15. Malak, O. A., Es-Salah-Lamoureux, Z., and Loussouarn, G. (2017) hERG S4-S5 linker acts as a voltage-dependent ligand that binds to the activation gate and locks it in a closed state. *Sci. Rep.* **7,** 113 CrossRef Medline
16. de la Peña, P., Machin, A., Fernández-Trillo, J., Domínguez, P., and Barros, F. (2013) Mapping of interactions between the N- and C-termini and the channel core in HERG K^+ channels. *Biochem. J.* **451,** 463–474 CrossRef Medline
17. Morais Cabral, J. H., Lee, A., Cohen, S. L., Chait, B. T., Li, M., and Mackinnon, R. (1998) Crystal structure and functional analysis of the HERG potassium channel N terminus: a eukaryotic PAS domain. *Cell* **95,** 649–655 CrossRef Medline
18. Wang, J., Trudeau, M. C., Zappia, A. M., and Robertson, G. A. (1998) Regulation of deactivation by an amino terminal domain in human ether-a-go-go-related gene potassium channels. *J. Gen. Physiol.* **112,** 637–647 CrossRef Medline
19. Wang, J., Myers, C. D., and Robertson, G. A. (2000) Dynamic control of deactivation gating by a soluble amino-terminal domain in HERG K^+ channels. *J. Gen. Physiol.* **115,** 749–758 CrossRef Medline
20. de la Peña, P., Alonso-Ron, C., Machín, A., Fernández-Trillo, J., Carretero, L., Domínguez, P., and Barros, F. (2011) Demonstration of physical proximity between the N terminus and the S4-S5 linker of the human ether-a-go-go-related gene (hERG) potassium channel. *J. Biol. Chem.* **286,** 19065–19075 CrossRef Medline
21. Barros, F., Pardo, L. A., Dominguez, P., Sierra, L. M., and de la Pena, P. (2019) New structures and gating of voltage-dependent potassium (Kv) channels and their relatives: a multi-domain and dynamic question. *Int. J. Mol. Sci.* **20,** 248 CrossRef
22. Tristani-Firouzi, M., Chen, J., and Sanguinetti, M. C. (2002) Interactions between S4-S5 linker and S6 transmembrane domain modulate gating of HERG K^+ channels. *J. Biol. Chem.* **277,** 18994–19000 CrossRef Medline
23. Choveau, F. S., Rodriguez, N., Abderemane Ali, F., Labro, A. J., Rose, T., Dahimène, S., Boudin, H., Le Hènaff, C., Escande, D., Snyders, D. J., Charpentier, F., Mérot, J., Baró, I., and Loussouarn, G. (2011) KCNQ1 channels voltage dependence through a voltage-dependent binding of the S4-S5 linker to the pore domain. *J. Biol. Chem.* **286,** 707–716 CrossRef Medline
24. Ke, Y., Hunter, M. J., Ng, C. A., Perry, M. D., and Vandenberg, J. I. (2014) Role of the cytoplasmic N-terminal Cap and Per-Arnt-Sim (PAS) domain in trafficking and stabilization of Kv11.1 channels. *J. Biol. Chem.* **289,** 13782–13791 CrossRef Medline
25. Fernández-Trillo, J., Barros, F., Machín, A., Carretero, L., Domínguez, P., and de la Peña, P. (2011) Molecular determinants of interactions between the N-terminal domain and the transmembrane core that modulate hERG K^+ channel gating. *PLoS One* **6,** e24674 CrossRef Medline
26. Ng, C. A., Hunter, M. J., Perry, M. D., Mobli, M., Ke, Y., Kuchel, P. W., King, G. F., Stock, D., and Vandenberg, J. I. (2011) The N-terminal tail of hERG contains an amphipathic α-helix that regulates channel deactivation. *PLoS One* **6,** e16191 CrossRef Medline
27. Long, S. B., Campbell, E. B., and Mackinnon, R. (2005) Voltage sensor of Kv1.2: structural basis of electromechanical coupling. *Science* **309,** 903–908 CrossRef Medline
28. Shen, H., Zhou, Q., Pan, X., Li, Z., Wu, J., and Yan, N. (2017) Structure of a eukaryotic voltage-gated sodium channel at near-atomic resolution. *Science* **355,** eaal4326 CrossRef Medline

29. Yan, Z., Zhou, Q., Wang, L., Wu, J., Zhao, Y., Huang, G., Peng, W., Shen, H., Lei, J., and Yan, N. (2017) Structure of the Nav1.4-β1 complex from electric eel. *Cell* **170,** 470–482.e11 CrossRef Medline
30. Ma, L. J., Ohmert, I., and Vardanyan, V. (2011) Allosteric features of KCNQ1 gating revealed by alanine scanning mutagenesis. *Biophys. J.* **100,** 885–894 CrossRef Medline
31. Osteen, J. D., Barro-Soria, R., Robey, S., Sampson, K. J., Kass, R. S., and Larsson, H. P. (2012) Allosteric gating mechanism underlies the flexible gating of KCNQ1 potassium channels. *Proc. Natl. Acad. Sci. U.S.A.* **109,** 7103–7108 CrossRef Medline
32. Vardanyan, V., and Pongs, O. (2012) Coupling of voltage-sensors to the channel pore: a comparative view. *Front. Pharmacol.* **3,** 145 Medline
33. Sun, J., and MacKinnon, R. (2017) Cryo-EM structure of a KCNQ1/CaM complex reveals insights into congenital long QT syndrome. *Cell* **169,** 1042–1050.e9 CrossRef Medline
34. Tomczak, A. P., Fernández-Trillo, J., Bharill, S., Papp, F., Panyi, G., Stühmer, W., Isacoff, E. Y., and Pardo, L. A. (2017) A new mechanism of voltage-dependent gating exposed by KV10.1 channels interrupted between voltage sensor and pore. *J. Gen. Physiol.* **149,** 577–593 CrossRef Medline
35. de la Pena, P., Domínguez, P., and Barros, F. (2018) Gating mechanism of Kv11.1 (hERG) K(+) channels without covalent connection between voltage sensor and pore domains. *Pflugers Arch.* **470,** 517–536 CrossRef Medline
36. Sale, H., Wang, J., O'Hara, T. J., Tester, D. J., Phartiyal, P., He, J. Q., Rudy, Y., Ackerman, M. J., and Robertson, G. A. (2008) Physiological properties of hERG 1a/1b heteromeric currents and a hERG 1b-specific mutation associated with Long-QT syndrome. *Circ. Res.* **103,** e81–e95 Medline
37. Goodchild, S. J., and Fedida, D. (2014) Gating charge movement precedes ionic current activation in hERG channels. *Channels (Austin)* **8,** 84–89 CrossRef Medline
38. Horton, R. M., Cai, Z., Ho, S. M., and Pease, L. R. (2013) Gene splicing by overlap extension: tailor-made genes using the polymerase chain reaction. *BioTechniques* **54,** 129–133 CrossRef Medline
39. Sokolova, O. S., Sha-breve]itan, K. V., Grizel′, A. V., Popinako, A. V., Karlova, M. G., and Kirpichnikov, M. P. (2012) Three-dimensional structure of human Kv10.2 ion channel studied by single particle electron microscopy and molecular modeling. *Bioorg. Khim.* **38,** 177–184 Medline
40. Gilchrist, A., Li, A., and Hamm, H. E. (2002) Gα COOH-terminal minigene vectors dissect heterotrimeric G protein signaling. *Sci. STKE* **2002,** pl1 Medline
41. Jouni, M., Si-Tayeb, K., Es-Salah-Lamoureux, Z., Latypova, X., Champon, B., Caillaud, A., Rungoat, A., Charpentier, F., Loussouarn, G., Baró, I., Zibara, K., Lemarchand, P., and Gaborit, N. (2015) Toward personalized medicine: using cardiomyocytes differentiated from urine-derived pluripotent stem cells to recapitulate electrophysiological characteristics of type 2 long QT syndrome. *J. Am. Heart Assoc.* **4,** e002159 Medline
42. Silva, J., and Rudy, Y. (2005) Subunit interaction determines IKs participation in cardiac repolarization and repolarization reserve. *Circulation* **112,** 1384–1391 CrossRef Medline
43. Papadopoulos, J. S., and Agarwala, R. (2007) COBALT: constraint-based alignment tool for multiple protein sequences. *Bioinformatics* **23,** 1073–1079 CrossRef Medline
44. Thouta, S., Sokolov, S., Abe, Y., Clark, S. J., Cheng, Y. M., and Claydon, T. W. (2014) Proline scan of the HERG channel S6 helix reveals the location of the intracellular pore gate. *Biophys. J.* **106,** 1057–1069 CrossRef Medline